Science of the Total Environment 927 (2024) 172184

Contents lists available at ScienceDirect

Science of the Total Environment

journal homepage: www.elsevier.com/locate/scitotenv

Comparison of perfluorooctane sulfonate (PFOS), perfluorooctanoic acid (PFOA) and perfluorobutane sulfonate (PFBS) removal in a combined adsorption and electrochemical oxidation process

Antoine P. Trzcinski [a,*], Kouji H. Harada [b]

[a] School of Agriculture and Environmental Science, University of Southern Queensland, West Street, 4350, Queensland, Australia
[b] Department of health and environmental sciences, Graduate school of Medicine, Kyoto University, Kyoto 606-8501, Japan

HIGHLIGHTS

- >100 μg/L PFOS was fully degraded at a current density of 28 mA/cm^2.
- Up to 98 % PFOA (C_0 = 45 μg/L) was degraded at 25 mA/cm^2.
- PFBS could not be adsorbed on GIC and degraded.
- Loss of 3–40 % efficiency when using real water matrix under similar condition
- 95 and 68 % PFOS and PFOA removal at 28 mA/cm^2 for 20 min in real water

GRAPHICAL ABSTRACT

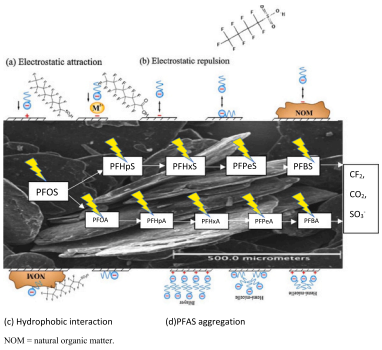

ARTICLE INFO

Editor: Baoliang Chen

Keywords:
PFOS
PFOA
PFBS
Adsorption
Graphite intercalated compound
Electro-chemical oxidation

ABSTRACT

This study focused on three of the most studied PFAS molecules, namely perfluorooctane sulfonate (PFOS), perfluorooctanoic acid (PFOA) and perfluorobutane sulfonate (PFBS). They were compared in terms of their adsorption capacity onto graphite intercalated compound (GIC), a low surface area, highly conductive and cheap adsorbent. The adsorption on GIC followed a pseudo second order kinetics and the maximum adsorption capacity using Langmuir was 53.9 μg/g for PFOS, 22.3 μg/g for PFOA and 0.985 μg/g for PFBS due to electrostatic attraction and hydrophobic interactions. GIC was added into an electrochemical oxidation reactor and >100 μg/L PFOS was found to be fully degraded (<10 ng/L) leaving degradation by-products such as PFHpS, PFHxS, PFPeS, PFBS, PFOA, PFHxA and PFBA below 100 ng/L after 5 cycles of adsorption onto GIC for 20 min followed by regeneration at 28 mA/cm^2 for 10 min. PFBS was completely removed due to degradation by aqueous electrons on GIC flakes. Up to 98 % PFOA was removed by the process after 3 cycles of adsorption onto GIC for 20 min followed by regeneration at 25 mA/cm^2 for 10 min. When PFBS was spiked individually, only 17 % was removed due to poor adsorption on GIC. There was a drop of 3–40 % by treating PFOS, PFOA and smaller sulfonates in a real water matrix under the same electrochemical conditions (20 mA/cm^2), but PFOS and PFOA removal percentage were 95 and 68 % after 20 min at 20 mA/cm^2.

* Corresponding author.
E-mail address: antoine.trzcinski@unisq.edu.au (A.P. Trzcinski).

https://doi.org/10.1016/j.scitotenv.2024.172184
Received 29 December 2023; Received in revised form 8 March 2024; Accepted 1 April 2024
Available online 2 April 2024

1. Introduction

PFAS (*per-* and polyfluoroalkyl substances) are anthropogenic chemicals displaying strong carbon fluorine bonds that provide unique properties, such as their resistance to heat, water, and oil. They are widely used in food packaging, lubricants, cosmetics and firefighting foams. PFOS (perfluorooctane sulfonate) is the most commonly used PFAS, but has been replaced by its shorter 4 carbon version PFBS in 2003 (Sundström et al., 2012). PFOA (perfluorooctanoic acid) specifically has been used in the production of non-stick cookware, water-repellent clothing, stain-resistant fabrics, and in certain firefighting foams, particularly those used at air bases and airports. PFOA is employed for polymerization in the manufacturing of various fluoropolymers, which have been applied in various industrial and consumer products such as Gore-Tex and Teflon (Mojiri et al., 2023). The widespread use of PFAS in various products and industrial processes has led to their presence in the environment, including water sources, soil, and even in the bodies of animals and humans. PFOS and PFBS was found to impair reproduction and alter offspring physiological function in *Caenorhabditis elegans* (Yue et al., 2020). Concerns about their persistence, potential health effects, and environmental impact have led to increased scrutiny and efforts to mitigate their presence and use in various applications. Elevated concentrations of PFOA (up to 120 $\times$ 10^6 ng/L), especially in wastewater, can result from industrial discharges, runoff from areas where PFAS-containing products are used, or improper disposal practices (Lei et al., 2022). PFBS was detected in drinking water at 10.7 ng/L in South Korea (Kim et al., 2020) and at 15 ng/L in Ireland (Harrad et al., 2019). The EPA health advisory level is currently fixed at 2000 ppt for PFBS (EPA, 2022). PFBS has also been detected at much higher levels in ground water from USA (9.25 μg/L) (Cui et al., 2020), and landfill leachate from China (80.22 μg/L) (Yan et al., 2015).

In 2016, the U.S. Environmental Protection Agency (EPA) issued a health advisory level of 70 ng/L for PFOA and PFOS combined in drinking water (EPA, 2016), but some states require a maximum PFOA level in drinking water at 14 ng/ L (Dadashi Firouzjaei et al., 2022). PFOA was found in Australian drinking water at ng L^{-1} levels in 44 % of all samples tested in South East Queensland (Thompson et al., 2011), but concentration in groundwater around army bases have been reported at μg/L levels. For instance, The average aggregate concentration of PFOS, PFOA, and PFHxS (perfluorohexanesulfonic acid) at an army site in Australia being reported as 4.92 μg/L signifies a notable presence of these PFAS in that particular environment (Leung et al., 2022).

Many existing technologies, like polymeric resins (Kothawala et al., 2017), reverse osmosis (Tang et al., 2006) and activated carbon (Szabo et al., 2017) are effective at capturing PFAS from water sources. However, these methods do not actually destroy PFAS molecules; instead, they transfer them to another phase or medium, which does present a risk of potential re-pollution if not managed properly. Thompson et al. (2011) even reported that the RO concentrate containing PFAS was released in a nearby river. Media such as activated carbon or resins must be incinerated or disposed of in landfills (Stoiber et al., 2020). Destruction technologies include sonolysis using ultrasonication (Cheng et al., 2008), microwave (Chou et al., 2013), alkaline hydrolysis (Hao et al., 2021), advanced oxidation processes (Vecitis et al., 2009) and supercritical water oxidation (Pinkard et al., 2021). In the case of treatment at 200 kHz under atmospheric air conditions for one hour, the removal rate for PFOA was reported as 28 %. Similarly, at a lower frequency of 20 kHz but for a longer duration of six hours, the removal rate for PFAS was recorded at 14.6 % (Lei et al., 2020). Microwave is the least effective method for PFOA degradation as 3.1–5 % removal efficiency was reported at a power in the range 90-140 W and temperature of 130 °C for 8–12 h (Lee et al., 2009; Chou et al., 2013). Photocatalysis was reported to remove up to 46 % PFOA in wastewater using zero-valent iron at acidic pH (Xia et al., 2022). Ozonation could remove up to 85 % PFOA in aqueous solutions under alkaline conditions (Lin et al., 2012). Tenorio et al. (2020) treated PFAS foams using UV activated sulphite reactions under alkaline environment and obtained 98 % and 93 % removal for PFOS and PFOA after 49 h, but short chain PFAS such as PFBS were still present. Li et al. (2023) used ultraviolet with sulphite to degrade PFOS but it was inefficient for PFBS. They developed a hybrid vacuum UV/sulphite/Iodide process which was found to degrade about 90 % PFBS due to the generation of aqueous e^- under alkaline conditions. It was found that this advanced reduced process can generate e^-_{aq} which can reductively convert C—F bond to C—H bond. There was also a higher degradation in the absence of oxygen because dissolved oxygen can easily eliminate reductive radicals such as e^-_{aq}. Plasma was also shown to be inefficient towards PFBS due to its poor hydrophobicity (Isowamwen et al., 2023), however, by adding a cationic surfactant which formed a complex with PFBS, up to 67 % PFBS was degraded at the plasma liquid interface due to solvated electrons (e^-_{aq}).

The electrochemical oxidation (EO) technique holds several advantages over traditional wastewater treatment processes. Its high energy efficiency, scalability, and modularity make it a promising method for treating wastewater. Unlike some other methods, EO can operate at ambient temperature and atmospheric pressure, reducing the need for energy-intensive conditions or specialized equipment. Additionally, its minimal reliance on chemicals earns it the label of "green technology," aligning with environmentally friendly practices. The simplicity of setting up and operating EO systems further contributes to its appeal as an efficient and eco-friendly wastewater treatment solution (Radjenovic et al., 2020). The application of electrochemical oxidation (EO) with low-cost graphene sponge electrodes, as reported by Duinslaeger and Radjenovic (2022), demonstrated 16.7 % to 67 % destruction of C4–C8 PFAS. Using boron-doped diamond (BDD) film electrodes, Liao and Farrell (2009) observed that between 44 and 70 % PFOA in wastewater was destroyed at 2.3–21.4 mA cm^{-2} (Liao and Farrell, 2009), while at 75 mA cm^{-2}, Pierpaoli et al. (2021) achieved 80 % removal of PFOA in landfill leachate.

The implementation of electrochemical oxidation (EO) on a large scale can indeed face challenges due to the complexity of manufacturing and associated costs. Electrodes play a crucial role in EO processes, and several anodes materials such SnO_2, BDD, PbO_2, TiO_2, Ti_4O_7 have shown promising results but potential issues such as a lower active surface area, the release of toxic heavy metals (in the case of some electrodes like PbO_2), surface fluorination, potential fragility leading to flaking of coatings, and a relatively short service life. The requirement for constant monitoring to determine when electrode replacement is necessary adds to operational complexity.

Using graphite intercalated compound (GIC) as a combined adsorbent and conductive material within an electrochemical system for PFAS removal presents an intriguing method. This method offers continuous regeneration of the adsorbent while applying an electric current, creating a synergistic adsorption and electrochemical oxidation (EO) process. The concept of electrosorption, where an electric field enhances the adsorption capacity of PFAS molecules, has been explored in various studies (Li et al., 2011). Even though there are numerous studies on the adsorption of PFAS or electrochemical oxidation of PFAS by electrodes, the combined adsorption and electrochemical oxidation of individual PFAS and PFAS mixture using GIC has not yet been explored in the literature. The comparison between long and short chain PFAS (i.e. PFOS and PFBS) as well as the comparison between perfluoro sulfonate and perfluoro carboxylic acids has not yet been investigated using this process. The removal efficiency in real environmental matrices is also often lacking from research studies on PFAS degradation. The aim of this paper was therefore to quantify the adsorption capacity of GIC towards individual PFAS, asses the degradation of three different PFAS through electrochemical oxidation and compare it the performance of the process using real environmental matrix.

2. Methods and materials

2.1. Adsorbent and adsorbate

Expandable graphite intercalation compound (GIC) in the form of flakes was obtained from Sigma-Aldrich (P/N: 808121). Perfluorooctane sulfonic acid (PFOS, $C_8HF_{17}KO_3S$, 538.15 g/mol) was purchased from Fluka (P/N: 77282). Perfluorooctanoic acid (PFOA, $C_8F_{15}OOH$, 414.2 g/mol) was purchased from Fluka (P/N: 77260, $\geq$ 90 % purity). Perfluorobutane sulfonic acid (PFBS, $C_4F_9KO_3S$, 338.19 g/mol) was purchased from Wako (P/N: 324–61491). Three different stock solutions containing approximately 10 mg/ L was prepared for each of the three studied compounds. Properties of these 3 PFAS are listed in supplementary material S1.

2.2. Batch adsorption tests

Batch adsorption experiments to evaluate the adsorption capacity of graphite for PFOS, PFOA and PFBS in separate experiments. The experiments were carried out in 250 mL Erlenmeyer flasks at a controlled temperature of 25 °C. To conduct the tests, a volume of 100 mL of deionized water containing 3 g of graphite was prepared. Various volumes of a stock solution containing PFOS, PFOA or PFBS were added to the flasks to achieve different initial concentrations. These flasks were then placed on an orbital shaker at 150 rpm to facilitate mixing and interaction between the graphite and the PFOA solution. Samples were withdrawn from the flasks at different time intervals to monitor the adsorption process until equilibrium was reached. To analyze the samples, they were filtered using a 0.22 μm filter to separate the graphite from the solution before analyzing the remaining concentration of PFOS, PFOA or PFBS. The amount of PFAS adsorbed at equilibrium, q_e (mg/ g) was calculated as:

$$q_e = \frac{C_o - C_e}{M} \text{ x V} \quad (1)$$

where, C_o and C_e (mg/ L) are the liquid-phase concentrations for initial sorbate and equilibrium, respectively. V is the volume of the solution (L) and M is the mass of graphite used. The Langmuir and Freundlich models were used to interpret the adsorption isotherms. The Langmuir model assumes monolayer adsorption on a surface with uniform sites, while the Freundlich model suggests heterogeneous adsorption onto a surface with multiple sites of varying energies (Mohammed et al., 2011). Kinetic models, such as pseudo first-order and pseudo second-order, were applied to describe the rate at which the adsorption process occurs over time (Trzcinski et al., 2011).

2.3. Electrochemical oxidation reactor

The reactor used to study the combined adsorption and regeneration of graphite is made of Perspex acrylic plastic in a Y-shape. Its technical drawings were reported elsewhere (Mohammed et al., 2012). Details of the experimental set up can be found somewhere else (Trzcinski and Harada, 2023). The catholyte compartment is approximately 500 mL tap water containing 3 % NaCl and HCl to pH between 1 and 2 (unless mentioned otherwise). About 100 g of graphite was added to fill the regeneration zone (12 cm deep and 5 cm thick). The volume of the reactor chamber is about 6 L, but only 3 L tap water was used for the experiments. The anodic and cathodic compartments were separated by a semipermeable Daramic Membrane (Daramic.com, USA). The current was adjusted using a digital power supply (0-3 A, 0-30 V, GPS-3030DD, Instek, Taiwan). First, an air pump was used to keep the graphite in suspension and promote adsorption for 20 min, then the pump was stopped, and the graphite was allowed to settle in the regeneration zone for 2 min, after which the current was switched on for 10 min.

2.4. Liquid-liquid extraction of PFAS compounds

The following procedure outlines the method used for the extraction and analysis of PFAS from a sample using a series of steps involving extraction, evaporation, and derivatization for analysis via gas chromatography–mass spectrometry (GC–MS). In a 2 mL Eppendorf centrifuge tube, a 200 μL sample was mixed with 200 μL of an ion-pairing buffer, in this case, Tetrabutylammonium hydrogensulfate. Then, 400 μL of methyl tert-butyl ether (MTBE) was added to extract all PFAS compounds. The tube was manually shaken to mix the contents thoroughly and then centrifuged at 5000 rpm for 3 min. After centrifugation, the MTBE layer, which contains the extracted PFAS, was carefully transferred to a glass tube. This extraction procedure was repeated 3 times to ensure all small chain PFAS were extracted. The MTBE in the glass tube was evaporated at 80 °C under a stream of nitrogen to remove the solvent and concentrate the extracted PFAS. 20 μL containing 1 ng of 11H-perfluoroundecanoic acid was added as internal standard to the concentrated sample and evaporated again. Derivatization was achieved using 200 μL of Bis(4-*tert*-butylphenyl)-iodonium hexafluorophosphate (BtBPI) in acetonitrile (1 % w v^{-1}) was then added to the glass tubes, and then transferred to a GC–MS vial for analysis.

2.5. GC–MS analysis

The analytical setup for the analysis of PFOA using gas chromatography–mass spectrometry (GC–MS) involved a DB-5MS capillary column (30 m long, 0.25 mm internal diameter, and 0.25 μm film thickness) installed in an Agilent 6890 GC-5973MSD instrument. The injection volume for the samples was set at 1 μL as described in (Harada et al., 2020). The coefficient of variance was 6 % ($n = 3$).

3. Results and discussion

3.1. Adsorption of PFOS, PFOA and PFBS using GIC

Fig. 1A shows the adsorption kinetics whereas Fig. 1B, C and D show the adsorption isotherms models fitted to the data of PFOS, PFOA and PFBS, respectively. The adsorption capacity was the highest for PFOS which reached 54 μg/g, followed by PFOA with 22.3 μg/g and PFBS with 2.6 μg/g. This is due to the higher hydrophobicity of longer PFAS. Despite the same length, PFOS is also more hydrophobic than PFOA due to the more hydrophilic head on PFOA which is consistent with many studies that studied the adsorption of PFAS onto activated carbons (Zhang et al., 2016). However, activated carbon can achieve significantly higher adsorption loadings: 15.8 mg/g, 10.3 and 7.5 mg/g for PFOS, PFOA and PFHpA, respectively (Zhang et al., 2016). The sorption equilibrium on GIC is relatively fast for PFOS which required 1–2 h, whereas PFOA and PFBS require only 20–60 min (Fig. 1A). This is significantly faster than activated carbons which require 24 h for PFOS and 120 h for PFOA and PFHpA (Zhang et al., 2016). It is worth noting that these adsorption capacities are higher than what can be achieved with biochar amended soil which has been reported to adsorb 0.025–0.139 μg PFOA g^{-1} and 0.094–0.223 μg PFOS g^{-1} (Askeland et al., 2020).

In order to better understand the factors controlling sorption rates, the kinetic data were fitted with pseudo first and second order kinetic models. The curves in Fig. 1A represent the pseudo second order kinetic model which fitted the data better than the first order kinetic model. The coefficients for both kinetic models are given in Table 1 where the estimated correlation coefficient ($R^2 = 0.99$) confirmed the better fit of the second order kinetic model for all 3 PFAS studied. The adsorption capacity at equilibrium (q_e) was found to be 56.18 μg/g for PFOS, 10.05 μg/g for PFOA and 3.85 μg/g through data fitting, which were close to the experimental data (53.92 μg/g for PFOS, 9.87 μg/g for PFOA and 3.75 μg/g for PFBS). The rate constant k_2 depends on the properties of the sorbate and sorbent and is inversely proportional to the sorption rate

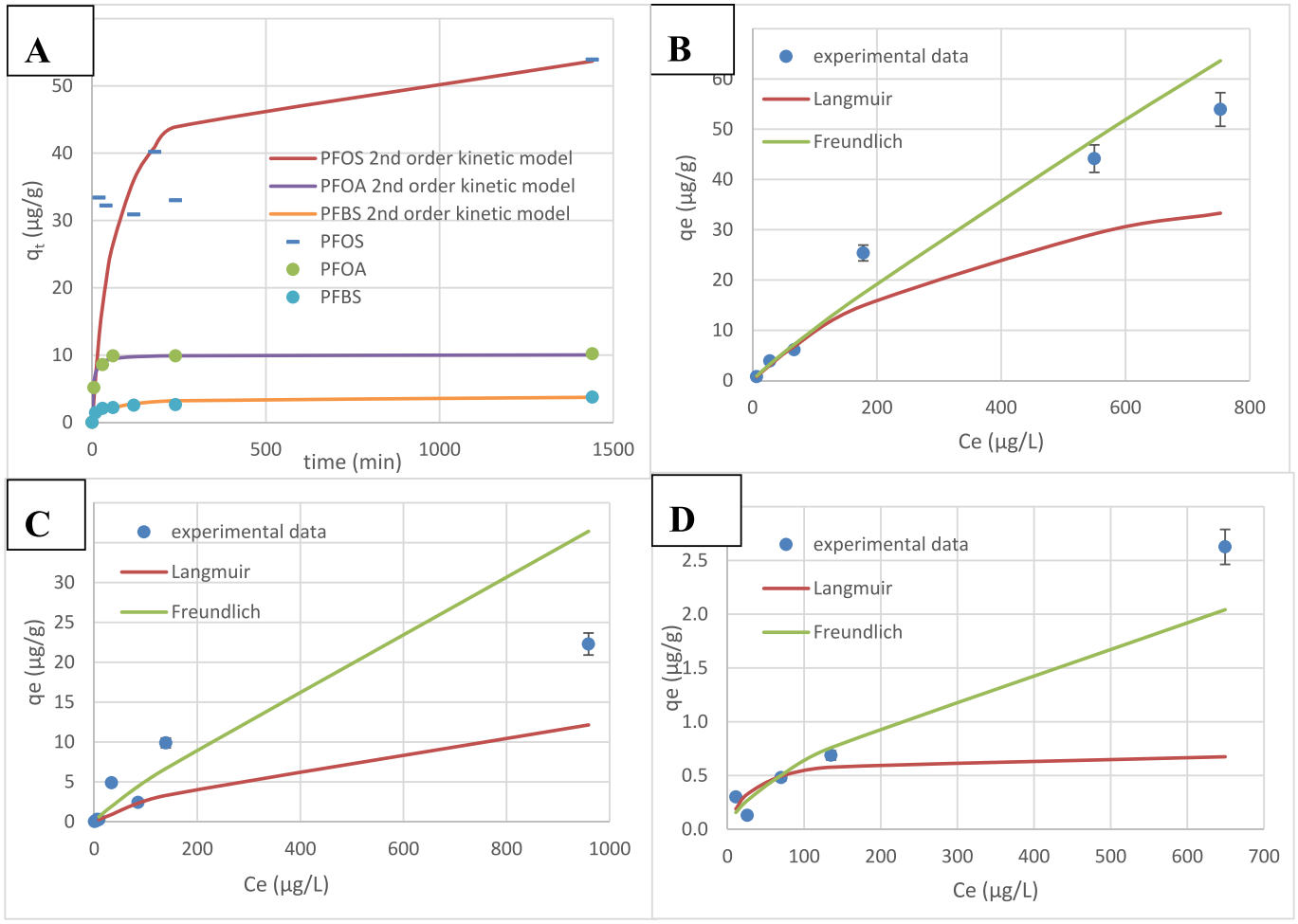

Fig. 1. (A) Pseudo- second order kinetic model (curve) fitted to the adsorption data (points) of PFOS, PFOA and PFBS. (B) Langmuir and Freundlich adsorption model fitted to the data of PFOS adsorption on GIC. (C) Langmuir and Freundlich adsorption model fitted to the data of PFOA adsorption on GIC. (D) Langmuir and Freundlich adsorption model fitted to the data of PFBS adsorption on GIC. The error bars represent the standard deviation ($n = 3$).

Table 1
Parameters of kinetic models fitted to the experimental data.

PFAS	Pseudo first-order			Pseudo second-order			
	k_1 (min^{-1})	q_{e1} (µg/ g)	R^2	k_2 (g $µg^{-1}$ min^{-1})	q_{e2} (µg/g)	h (µg/ g min^{-1})	R^2
PFOS	0.0062	30.6	0.3430	0.0002	56.18	0.771	0.9899
PFOA	0.1437	9.1319	0.9556	0.0261	10.0503	0.435	0.9970
PFBS	0.009	2.3953	0.6312	0.0051	3.8521	0.076	0.9963

(Zhang et al., 2016). The rate constants were found to be 0.0002, 0.0261 and 0.0051 g $µg^{-1}$ min^{-1} for PFOS, PFOA and PFBS, respectively, which confirms the higher sorption rate of PFOS, followed by PFBS, then PFOA. The coefficient h in Table 1 represents the initial sorption rate when $t = 0$ and can be calculated as $k_2.q_e^2$. It was found that the h value for PFOS was 10 times that of PFBS confirming the higher electrostatic attraction of PFOS for GIC due to a higher hydrophobicity. The initial sorption rate of PFOA was 0.435 µg/ g min^{-1} due to PFOA being less hydrophobic than PFOS because PFOS has one more carbon-fluorine bond in its perfluoroalkyl chain (Li et al., 2011). The pseudo second order model assumes that the rate-limiting step involves chemisorption, which encompasses electron sharing or exchange between the sorbent (GIC) and sorbate (PFAS) (Sharma and CF Forster, 1996). The finding that the pseudo-second order rate model fits well our data suggests that there might indeed be electronic interactions happening between PFAS and GIC. This could imply a stronger chemical bonding or exchange of electrons between these substances during the adsorption process, reinforcing the idea that the rate-limiting step involves chemisorption.

Previous studies have highlighted the significance of electrostatic interactions in the sorption of PFOA and PFOS to GAC (Deng et al., 2015).The observation that PFOS exhibits greater sorption both in terms of rate and quantity despite having the same carbon chain length as PFOA suggests that the hydrophilic head group present in PFAS significantly influences their sorption behavior on GIC. The differences in sorption between PFOS and PFBS, despite reaching equilibrium within the same timeframe, can be attributed to their varying degrees of hydrophobicity. The results comparing PFOS and PFBS show that hydrophobicity plays a pivotal role in the interaction between these compounds and the GIC surface. Our results are surprisingly similar to (Wang et al., 2015) who showed a high sorption capacity for PFOS on boehmite, while almost no PFBS was adsorbed suggesting that hydrophobic interactions was dominant on boehmite and GIC.

The sorption isotherms of PFOS, PFOA and PFBS are shows in Fig. 1B, C and D, respectively. Langmuir and Freundlich coefficients were calculated using the linearization method and are shown in Table 2. It can be seen that Langmuir model represented PFOS and PFOA adsorption better than Freundlich model, whereas PFBS was not well represented by neither of the models. This can be attributed to the fact that PFBS was not adsorbed by GIC. The Freundlich constant K_F represents the adsorption capacity which followed the order PFOS > PFOA > PFBS. The higher value of 1/n for PFOA indicates a more homogenous distribution of the adsorption site energies. Langmuir model can predict the maximum adsorption capacity of GIC which was higher for PFOS (53.93 μg/g) than PFOA (22.28 μg/g). PFOS, PFBS and PFOA also form an anion at a wide range of pHs which can explain the electrostatic interactions. Lower pH can increase the positive charges on GIC, increasing the adsorption potential for PFBS, but adsorption was insignificant in this study even at pH 4. Even though initial concentrations were similar for the 3 PFAS, the equilibrium concentrations were smaller for PFOS demonstrating a better affinity towards GIC. Given the better fit with Langmuir, monolayer adsorption on homogeneous GIC is more likely and the data for PFOS showed that some desorption could have taken place which indicates that chemical bond with GIC was unlikely. It is more likely that the preferred mode of adsorption was through electrostatic attraction and hydrophobic interaction with GIC. Aggregation through bilayer and hemimicelle is also possible, but only at concentration greater than at least 0.001 % of the critical micelle concentration (CMC) (Du et al., 2014). Harada et al. (2005) reported a CMC for PFOS and PFOA of 8 mM and 25 mM, respectively, indicating that micelles were not formed, but that hemimicelle formation were plausible for PFOS and PFOA in the current study. Increased hydrophobicity due to longer perfluoro chains promotes the formation of surface aggregates and the potential for PFOS aggregates was therefore much stronger than for PFBS.

3.2. Electro-chemical oxidation of PFOS

In this experiment, 3 mL of the PFOS stock solution was spiked into the electrochemical oxidation reactor after each adsorption and regeneration cycle to investigate the removal of PFOS and potential accumulation of PFOS breakdown by-products. It is important to note that unlike most electrochemical oxidation studies, the reactor was spiked multiple times as shown by the red arrow in Fig. 2A, not just at time 0. Fig. 2A shows the concentration of PFOS after each adsorption and regeneration step of each cycle, while Fig. 2b shows the concentration of PFOS degradation by-products, i.e. PFHpS, PFHxS, PFPeS, PFBS, PFOA, PFHxA and PFBA. At a current density of 28 mA/cm^2, PFOS removal was 98.9 % after the first cycle demonstrating a remarkable efficiency towards PFOS. The concentration dropped further below the detection limit of the instrument (< 10 ng/L) after cycle 5. PFHxS was the main by-product with a concentration of 10.5 μg/L, but it decreased to non-detectable levels (< 10 ng/L) after the first cycle. Similarly, PFHpS, PFPeS and PFBS were detected respectively at 343 ng/L, 240 ng/L and 109 ng/L (Fig. 2B), but decreased further to non-detectable levels after the first cycle, demonstrating the high efficiency of the process towards PFOS and smaller perfluoro sulfonates. It is worth noting that PFBS was completely removed to non detectable levels in this experiment which is somewhat unexpected because it was found that its adsorption capacity on GIC was very limited (Fig. 1D). The results imply therefore that PFOS remained adsorbed on GIC until it was fully degraded. Because the current density was sufficient, all adsorption sites were regenerated to make place for additional PFOS which remains adsorbed and degraded while adsorbed on GIC flakes. The degradation taking place is known to be due to a combined action of hydroxyl radicals, e^-_{aq} and electrochlorination but the exact contribution of each and preferred point of action is not known. Chlorine can also react with hydroxyl radicals to generate primary and secondary radicals such as $Cl^\bullet$, $ClOH^{\bullet-}$, $Cl_2^{\bullet-}$ but these are known to be inefficient towards PFBS (Zhang et al., 2022). PFBS is notoriously hard to degrade compared to PFOS and previous research showed that alkaline ultraviolet coupled with sulphite and iodide could generate e^-_{aq} that could convert C—F bond to C—H bonds in PFBS (Li et al., 2023). This suggest that e^-_{aq} were produced at the surface of GIC particles when the current is applied and that PFBS was degraded on GIC before it could desorb. If PFBS had desorbed in the bulk solution, its degradation would not have been possible because high dissolved oxygen concentration would have likely inhibited e^-_{aq} species.

It is known that PFOS can also break down to form PFOA which in turn breaks down to smaller perfluoro carboxylic acids such as PFHpA, PFHxA, PFPeA, PFBA, etc. Fig. 2B also shows that PFOA could be degraded as its concentration decreased from 91 ng/L to 26 ng/L, but smaller perfluoro carboxylic acids such as PFHxA and PFBA were found to accumulate slowly in the reactor to 95 ng/L and 83 ng/L after 5 cycles, respectively, indicating that smaller perfluoro carboxylic acids were more difficult to adsorb onto GIC due to being less hydrophobic than longer chain PFAS. This accumulation was also due to the multiple PFOS spikes in the reactor which constantly produced smaller by-products. During the degradation of PFOS, it was also revealed that short-chain perfluoro sulfonates were easier to remove than the corresponding short-chain perfluoro carboxylic acids under the same conditions, possibly due to desorption.

When the generation of e^-_{aq} is dominant compared to other reactive oxygen species such as $^\bullet OH$, H_2O_2, O_3, $^\bullet O_2^-$ and H_3O^+, the degradation of PFOS via one-electron transfer mechanism become dominant due to e^-_{aq} high reduction potential of −2.9 V (Deng et al., 2021). When an electric field is applied, an electron from PFOS is initially transferred to the anode to form a PFOS radical according to the following reaction:

$$C_8F_{17}SO_3^- \rightarrow {}^\bullet C_8F_{17}SO_3 + 1e^-$$

The radical would then decompose according to:

$$^\bullet C_8F_{17}SO_3 + H_2O \rightarrow {}^\bullet C_8F_{17} + SO_4^{2-} + 2H^+$$

Subsequently, $^\bullet C_8F_{17}$ will react with hydroxyl radicals to undergo a stepwise elimination of CF_2 subunits (Deng et al., 2021). According to that mechanism, after the C—S scission of $^\bullet C_8F_{17}SO_3^{2-}$, it will decompose into $C_8F_{17}^-$ followed by the production of $C_8F_{17}OH$, which is subsequently converted to PFOA (Gu et al., 2016). On the other hand, $^\bullet C_8F_{17}$ may be formed in the desulfonation reaction, before being transformed to PFOA (Bentel et al., 2019). It can be seen in Fig. 2B that PFOA was indeed produced from the degradation of PFOS which confirms the degradation pathway during the combined adsorption and electrochemical oxidation process using GIC. In the first pathway, $^\bullet C_8F_{17}$ will react with hydroxyl radicals to yield $C_8F_{17}OH$ which will then decompose into HF and $C_7F_{15}CFO$. The latter will then hydrolyze into $C_7F_{15}COO^-$, HF and H^+. This leaves us with a carboxylic acid which will undergo successive steps: firstly, Kolbe decarboxylation (releasing -CO_2), radical reaction involving $^\bullet OH$, intramolecular rearrangement (releasing -HF) and hydrolysis (releasing -HF) to get rid of one CF_2 unit (Niu et al., 2012). The same cycle is then repeated until PFCAs are finally mineralized to CO_2 and HF. In the second pathway with an excess of oxygen, the radical $C_8F_{17}OO^\bullet$ is produced. It can react with other radicals with a general form of $RFOO^\bullet$ to yield $C_8F_{17}O^\bullet$, $RFO^\bullet$ and O_2. $C_8F_{17}O^\bullet$ will then decompose into $C_7F_{15}^\bullet$ and COF_2. The latter will

Table 2
Parameters for the adsorption models of PFOS, PFOA and PFBS adsorption onto GIC.

Sorbate	Langmuir			Freundlich		
	K_L (μg/g)	b_L (L μg^{-1})	R^2	K_F (μg$^{1-1/n}$ L$^{1/n}$ g^{-1})	n	R^2
PFOS	53.9	0.002	0.99	0.1612	1.108	0.981
PFOA	22.3	0.0012	0.9951	0.044	1.011	0.935
PFBS	0.985	0.025	0.4271	0.029	1.372	0.875

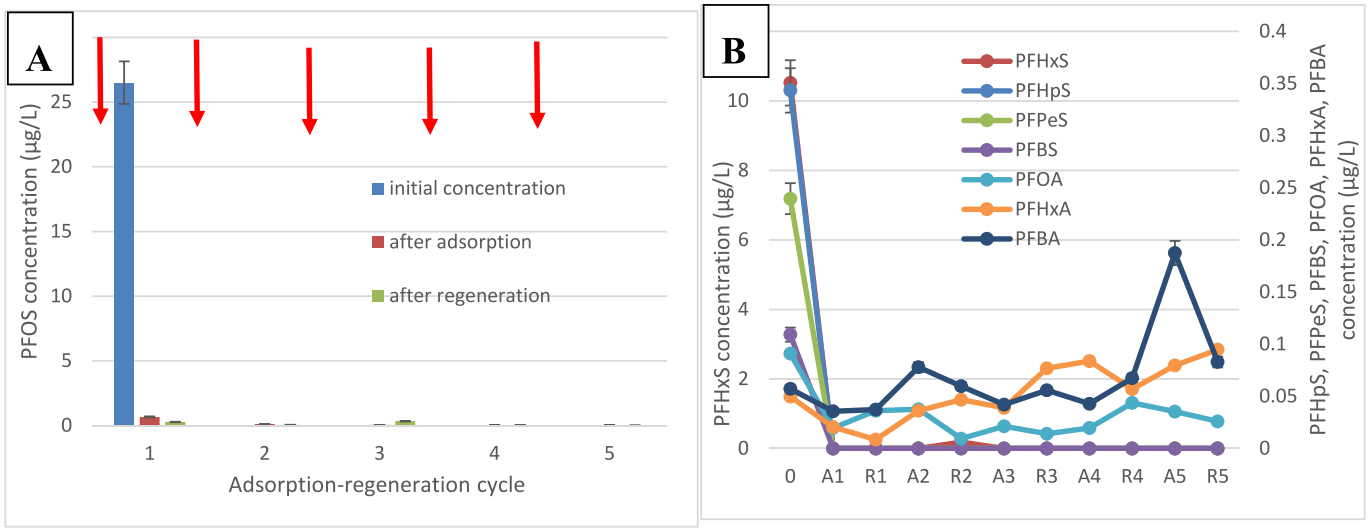

Fig. 2. (A) Time dependence of PFOS concentration in tap water after 5 cycles of adsorption onto GIC for 20 min followed by regeneration at 28 mA/cm^2 for 10 min. The red arrow represents a 3 mL spike of PFOS stock solution into the electrochemical reactor (B) Time dependence of PFHpS, PFHxS, PFPeS, PFBS, PFOA, PFHxA and PFBA concentration in water after each adsorption step (denoted by the letter A) and regeneration step (denoted by the letter R).

hydrolyze into CO_2 and HF. The radical $C_7F_{15}^{\bullet}$ will then undergo the same pathways until complete defluorination.

3.3. Electro-chemical oxidation of PFOA

Fig. 3A shows the degradation of PFOA at a current density of 25 mA/cm^2 after multiple spikes and the PFOA concentration dropped from 14.8 µg/L to 281 ng/L after the first cycle achieving a remarkable 98 % removal. However, the concentration slightly increased after the third cycle to 449 ng/L indicating an incomplete removal and saturation of GIC active sites after the second and third PFOA spike. The degradation of PFOA was confirmed by Fig. 3B showing the presence of PFHpA at a concentration of 2.687 µg/L stabilizing to 0.9 µg/L after 3 cycles. PFBA was also detected up to 282 ng/L and was not fully removed. Interestingly, PFHxA and PFPeA were not detected under these experimental conditions. The higher concentration of perfluoroheptanoic acid (PFHpA) observed during the degradation process implies that the breakdown of PFHpA might have been the limiting factor in the electrochemical oxidation of perfluorooctanoic acid (PFOA) on the graphite intercalation compound (GIC). The results suggest that PFOA and smaller perfluorocarboxylic acids (PFCAs) degradation requires more GIC and longer regeneration time than PFOS. The fact that smaller PFCAs are more difficult to degrade is consistent with Niu et al. (2012) who also obtained a PFOA half-life of approximately 15 min, but we went further by spiking the reactor a second and third time, and we showed that GIC could be regenerated in situ by electrochemical oxidation without affecting the performance after the second and third successive spike. This observation implies that as PFOA and its by-products underwent degradation, more adsorption sites on the graphite became available during successive regeneration cycles. Consequently, the decrease in concentration observed in the water samples suggests that PFOA and its by-products remained adsorbed on the graphite surface until they underwent breakdown or degradation. This indicates a dynamic process wherein the adsorbed compounds remained attached to the GIC until they were effectively degraded, without leaching or desorbing back into the water over time.

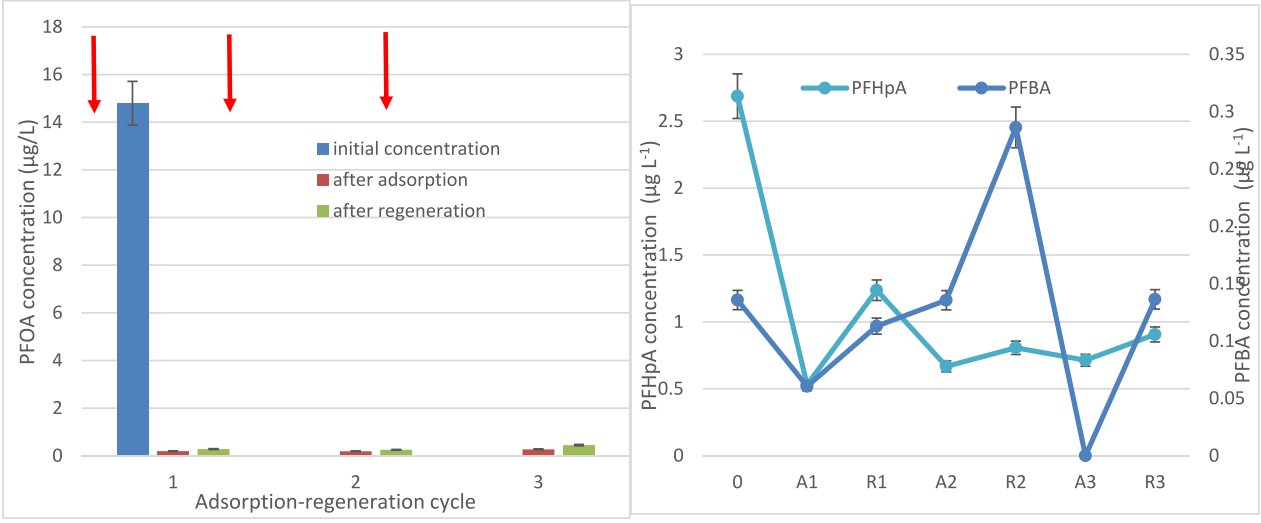

Fig. 3. (A) Time dependence of PFOA concentration in tap water after 3 cycles of adsorption onto GIC for 20 min followed by regeneration at 25 mA/cm^2 for 10 min. The red arrow represents a 3 mL spike of PFOA stock solution into the electrochemical reactor (B) Time dependence of PFHpA, and PFBA concentration in water after each adsorption step (denoted by the letter A) and regeneration step (denoted by the letter R).

The proposed process for the adsorption, removal, and degradation of PFOA involves several mechanisms that operate in tandem. Firstly, when GIC immersed in an electrolyte solution is subjected to an external electrostatic field, the particle surfaces acquire either a positive or negative charge (Zhang et al., 2013). This charge on the GIC surfaces leads to an electrostatic attraction between the charged PFOA anions and the oppositely charged GIC flakes, resulting in a phenomenon known as electrosorption. This process combines the adsorption facilitated by the hydrophobic nature of PFOA with electrosorption, effectively enhancing the removal of PFOA onto the GIC surface. This decrease in pH, especially in the absence of alkalinity, occurs due to a combination of factors. Acid diffusion through the membrane and the generation of acid at the anode contribute to this pH drop (Mohammed et al., 2011). The resulting acidic medium creates conditions conducive to the acquisition of a positive charge by PFOA molecules. These positively charged PFOA molecules are then attracted to the negatively charged sides of GIC flakes or the negatively charged electrode.

The electrochemical oxidation process involves the generation of hydroxyl radicals ($^{\bullet}OH$) and electron transfer reactions, playing key roles in the degradation of perfluorooctanoic acid (PFOA). However, hydroxyl radicals alone might have limitations in breaking the strong C—F bonds present in PFOA molecules (Ambaye et al., 2022). When the generation of hydrated electrons (e^-_{aq}) is predominant compared to other reactive oxygen species, such as hydroxyl radicals, hydrogen peroxide, ozone, superoxide radicals, and hydronium ions, the degradation of PFOA primarily occurs via a one-electron transfer mechanism due to e^-_{aq} high reduction potential of −2.9 V (Deng et al., 2021). This electron transfer results in the conversion of the PFOA anion ($C_7F_{15}COO^-$) into radicals ($C_7F_{15}COO^{\bullet}$). Subsequent steps involve Kolbe decarboxylation, radical reactions, intramolecular rearrangements, and hydrolysis, gradually breaking down the PFOA molecules into shorter-chain perfluorocarboxylic acids (PFCAs) (Niu et al., 2012). In oxygen-rich environments, reaction pathways involve the interaction of C_7F_{15} with oxygen, leading to the formation of radicals like $C_7F_{15}O^{\bullet}$ and ultimately resulting in the breakdown of PFOA molecules into smaller fragments, including CF_2O, C_6F_{13}, and CO_2. In hydroxyl radicals rich environments, C_7F_{15} can transform into $C_7F_{15}OH$, leading to the formation of $C_7F_{15}O^{\bullet}$, which follows a similar sequence of reactions resulting in the degradation of PFOA into smaller components, eventually leading to the production of CO_2 and HF. The presence of PFOA by-products in the experiment confirms these proposed degradation pathways. It suggests that hydrated electrons (e^-_{aq}) also play a role in the process, contributing to defluorination and scission of the centermost C—C bonds in PFOA molecules (Gu et al., 2016). This series of reactions eventually leads to the breakdown and mineralization of PFOA and its by-products into smaller, less persistent compounds and, ultimately, to CO_2 and HF.

3.4. Electro-chemical oxidation of PFBS

In Fig. 4, a single 3 mL spike of the PFBS stock solution was pipetted into 3 L of tap water, a sample was taken, and the spiked water was then poured into the reactor and 5 consecutives cycles of adsorption and regeneration at 43 mA/cm^2 were carried out. It can be seen that PFBS was hardly removed by physical adsorption, electrostatic attraction onto GIC, electrosorption nor by electrochemical regeneration of GIC. The GC–MS used in this study could unfortunately not detect PFAS with fewer than 4 carbons. Only 17 % PFBS was removed by the process even at a relatively higher current density of 43 mA/cm^2. This is consistent with Fig. 1A and D which showed that PFBS could barely be adsorbed onto GIC. However, this contradicts Fig. 2B which showed that PFBS could be totally removed when it appeared as a degradation by-products of PFOS because PFOS can be adsorbed first onto GIC, and all subsequent by-products remain adsorbed on GIC and are degraded before they have time to desorb into the bulk . This shows that the electrochemical oxidation of PFBS works only when the PFBS molecules are already adsorbed onto GIC which is where the degradation takes place. It also

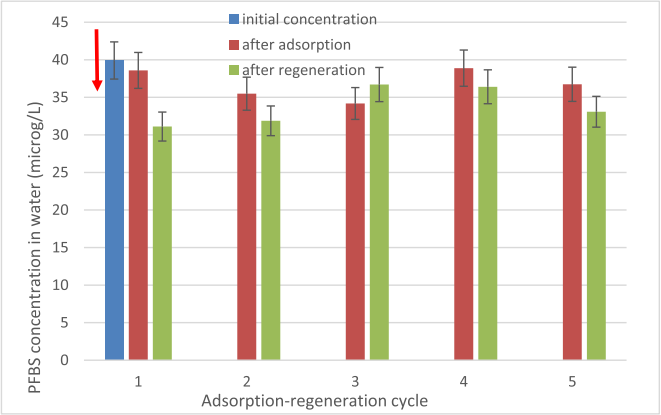

Fig. 4. (A) Time dependence of PFBS concentration in tap water after 5 cycles of adsorption onto GIC for 20 min followed by regeneration at 43 mA/cm^2 for 10 min. The red arrow represents a 3 mL spike of PFBS stock solution into the electrochemical reactor.

strongly suggests that $OH^{\bullet}$ radicals produced in the bulk are inefficient towards PFBS and that only hydrated electrons (e^-_{aq}) produced at the surface at GIC or anode can degrade PFBS if it appears as a by-product of adsorbed PFOS, but not when it is spiked as PFBS because it will not adsorb onto GIC. This demonstrates that different mechanisms are responsible for PFOS and PFBS breakdown in the electrochemical oxidation process using GIC, and that different processes are therefore required for the full degradation of PFAS: electrochemical oxidation of long chain PFAS at acidic pH followed by an advanced reduced process involving hydrated electrons (e^-_{aq}) at alkaline pH for small chain PFAS. Alternatively, novel adsorbent which can effectively adsorb long and short chain PFAS must be developed. These novel adsorbents should have large surface area to maximize adsorption and high electrical conductivity in order to produce large quantities of hydroxyl radicals and hydrated electrons (e^-_{aq}) when a small electrical current is applied.

3.5. Electro-chemical oxidation of a mixture of PFOS, PFOA and PFBS

In this experiment, a single spike of PFOS, PFOA and PFBS was injected in the water before taking a sample and turning on the air pump and the power supply at the same time. By doing so, contaminants are mixed with GIC to promote adsorption while they can be degraded when the GIC is in the regeneration zone. Despite the air bubbles present in the regeneration zone, a current density of 20 mA/cm^2 was still possible. Fig. 5A shows a reduction of 83 % and 62 % for PFOS and PFOA, respectively, while only 11 % PFBS was removed. The lower removal can be explained by the competition between PFOS and PFOA for the adsorption sites of GIC. Liang et al. (2018) also observed higher removal of PFOS (91 %) compared to PFOA (32 %) when using a Ti_4O_7 anode, indicating that there is a strong relationship between hydrophobicity of PFAS and anode which affect mass and electrons transfer in the electrochemical oxidation process.

Fig. 5B shows that PFHxS was the dominant by-products but its concentration decreased from 14 to 4.43 μg/L (68 % removal). All the other by-products were detected below 300 ng/L. Among them, PFHpS decreased by 78 % and PFPeS by 33.7 %. It is clear that the smaller the perfluoro sulfonic acid chain, the lower the removal efficiency of the process. With regards to the perfluoro carboxylic acids, PFHxA concentration decreased by 36 %, while the concentration of PFHpA and PFBA increased during the simultaneous adsorption and regeneration.

3.6. Electro-chemical oxidation of a mixture of PFOS, PFOA and PFBS in real water matrix

The same experiment was repeated in a real water matrix taken from

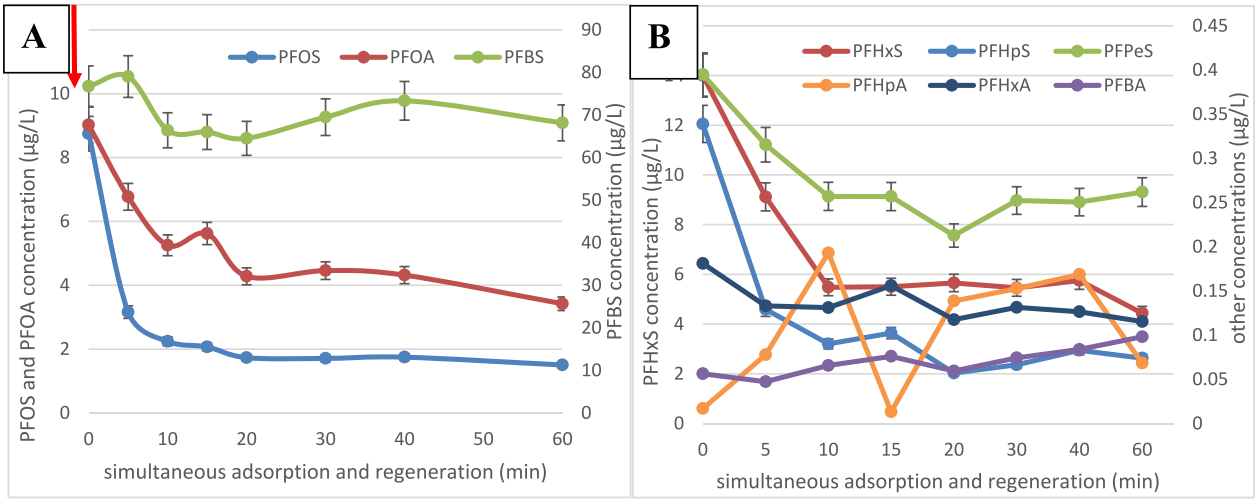

Fig. 5. (A). Time dependence of PFOS, PFOA and PFBS concentration in tap water during the simultaneous adsorption and regeneration process at 20 mA/cm^2. The red arrow represents a 3 mL spike of PFOS, PFOA and PFBS stock solution into the electrochemical reactor. (B) Change in the concentration of smaller chain perfluoro sulfonic acids and perfluoro carboxylic acids during the simultaneous adsorption and regeneration process.

a local pond (Heian Shrine, Kyoto, Japan). The water had the characteristics listed in Table S2. Despite being relatively clear, the water tested positive for *E. coli* and contained organic matter as shown by a TOC content of 2.2 mg/L and suspended matter content of 2.6 mg/L. The colour and turbidity indicated the possibility of natural organic matter such as humic and fulvic acids being also present.

In this experiment using a real water matrix, the removal of PFOS and PFOA dropped to 56 % and 51 %, respectively, whereas the concentration of PFBS increased notably which is due to the degradation of PFOS to PFBS (Fig. 6A). This can be explained by the competition with natural organic matter for electrosorption on GIC, and as a result more PFOS remained unadsorbed or adsorbed on natural organic matter instead of GIC, while still being degraded by hydroxyl radicals in the bulk solution to smaller perfluoro sulfonates and carboxylic acid which also remained in bulk. It is also possible that PFBS desorbed from GIC due to competition with natural organic matter. The removal of PFHpS, PFHxS and PFPeS was 75 %, 34 % and − 9 % indicating that the process was less effective in real water matrix. There was a drop of 3–40 % by treating PFOS, PFOA and smaller sulfonates in a real water matrix under the same electrochemical conditions (20 mA/cm^2). This can be explained by coexisting anions such as NO_3^-, NO_2^-, HCO_3^-, Br^- and dissolved organic matter(Li et al., 2023) and carbonate hardness (Sukmilin and Sangsirimongkolying, 2021) that are all scavengers of hydroxyl radicals. Moreover, Barisci and Suri (2020) also observed a reduced defluorination rate in long-chain PFAS (C > 7) in river water compared to deionized water due to these radical scavengers. Adsorption of PFAS on GIC was also affected by the competition with these anions for positively charged sites on GIC. PFHpA, PFHxA and PFBA removal percentages were 100 %, 18 % and 41 %, respectively, which was better than what was achieved in tap water (Fig. 5B). However, the final concentrations were similar in both matrices.

Finally, Fig. 7A and B shows the same experiment in real water matrix, but by applying adsorption and regeneration sequentially instead of simultaneously. This allows us to achieve a higher current density of 40 mA/cm^2 as the GIC is allowed to settle down in the regeneration zone for 2 min before applying the current for 20 min. It can be seen that PFOS and PFOA removal percentage were 95 and 68 % which is slightly better than in tap water, but in order to achieve this, the

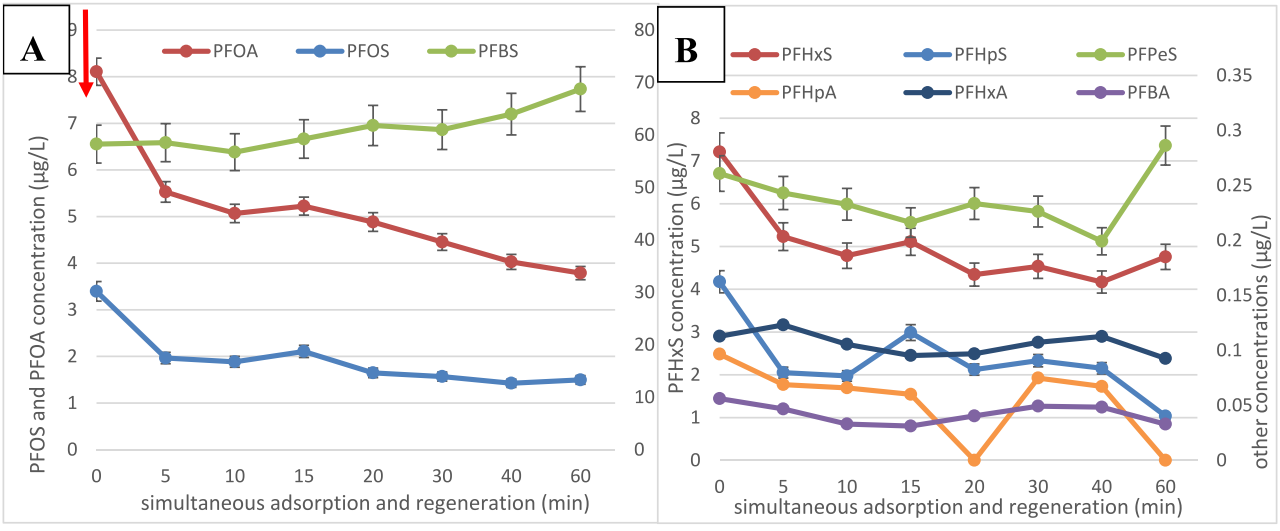

Fig. 6. (A). Time dependence of PFOS, PFOA and PFBS concentration in real environmental water matrix during the simultaneous adsorption and regeneration process at 20 mA/cm^2. The red arrow represents a 3 mL spike of PFOS, PFOA and PFBS stock solution into the electrochemical reactor. (B) Change in the concentration of smaller chain perfluoro sulfonic acids and perfluoro carboxylic acids during the simultaneous adsorption and regeneration process.

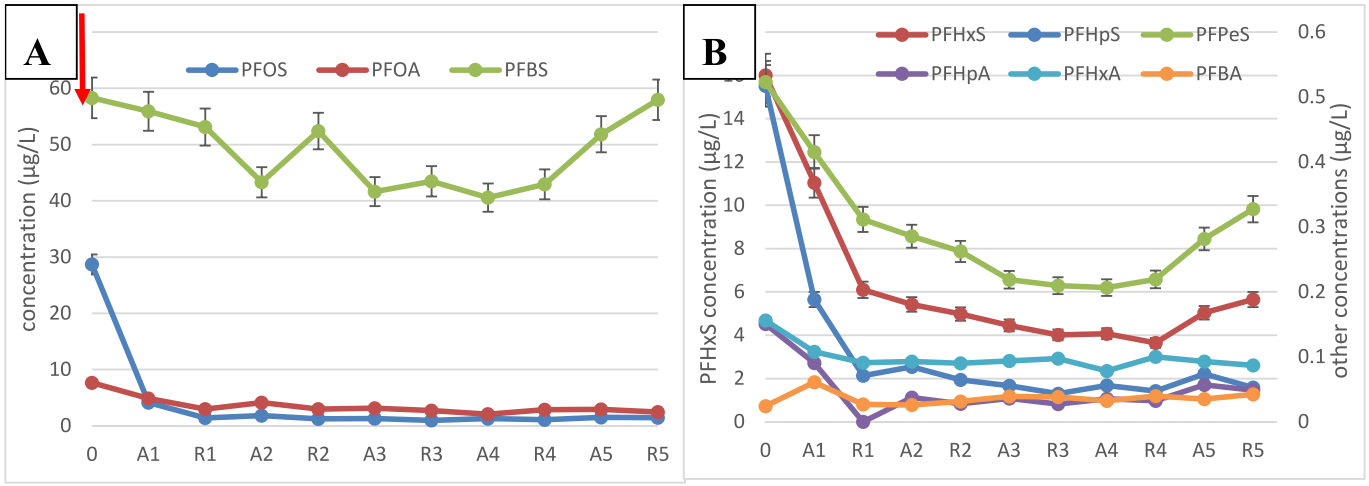

Fig. 7. (A) Time dependence of PFOS, PFOA and PFBS concentration in real environmental water matrix after 5 cycles of adsorption onto GIC for 20 min followed by regeneration at 40 mA/cm^2 for 20 min. The red arrow represents a 3 mL spike of PFOS, PFOA and PFBS stock solution into the electrochemical reactor (B) Time dependence of PFHpS, PFHxS, PFPeS, PFHpA, PFHxA and PFBA concentration in real environmental water matrix after each adsorption (denoted by the letter A) and regeneration step (denoted by the letter R).

current density was doubled from 20 to 40 mA/cm^2 and the regeneration time was also doubled from 10 to 20 min. These operational conditions corresponded to an energy consumption of 13 kWh/m^3 which is significantly lower that what has been reported with ultrasonication: 1475 kWh/m^3 (Lin et al., 2016), sonolysis: 4045 kWh/m^3 (Moriwaki et al., 2005), photodegradation-boiling: 1177 kWh/m^3 (Lyu et al., 2015), microwave-hydrothermal: 2599 kWh/m^3 (Lee et al., 2009), photocatalysis/Fenton: 171 kWh/m^3 (Ohno et al., 2014) and UV/KI methods: 95 kWh/m^3 (Qu et al., 2010). But it is higher than 5–7 kWh/m^3 obtained with Ti_4O_7 reactive electrochemical membrane anode (Le et al., 2019).

PFBS concentration was found to decrease from 58 to 40.5 µg/L, but started to increase again after cycle 4 due to the degradation of PFOS by-products. This is consistent with Maldonado et al. (2021) who also observed an increase in short chain PFAS during the treatment of landfill leachate at 200 mA/cm^2 due to the unzipping mechanisms reported in the literature whereby a -CF_2 unit is released during the break down of PFAS until smaller PFAS are obtained. This demonstrates that electrochemical oxidation is not adapted to short-chain PFAS such as PFBS. The bottleneck of the process is therefore the adsorption and electrochemical oxidation of 4 carbon PFAS which would require a conductive adsorbent with higher affinity for more hydrophilic PFAS.

Fig. 7B shows the evolution with time of PFOS and PFOA breakdown by-products. Again, higher removal percentages were achieved with longer chains: PFHpS (89.8 %) > PFHxS (64.7 %) > PFPeS (37.4 %) > PFBS (0.6 %). In multi-compounds solutions of PFAS, Wang et al. (2020) also observed that long chain PFAS are degraded faster than short chain PFAS with the same functional headgroup. Moreover, perfluoro carboxylic acids of the same carbon chain length were degraded slower that perfluoro sulfonates.

These percentages were higher (PFHpS, PFPeS) or similar (PFHxS) than those obtained in tap water, demonstrating that high removals can be achieved in environmental matrix, but it required higher energy input and longer treatment time. PFHpA and PFHxA removal percentages were 67.6 % and 44.2 %, which was significantly better than during the simultaneous adsorption and regeneration experiment in tap water (Fig. 5B). PFBA concentration increased by 43 % showing again that smaller by-products are more difficult to remove in this process even at higher energy input and longer treatment time.

4. Conclusions

The adsorption of PFOS, PFOA and PFBS onto GIC occurred rapidly within 2 h. With a maximum adsorption capacity of 53.9 and 22.3 µg/ g for PFOS and PFOA, respectively. With 0.985 µg/ g GIC, PFBS was barely adsorbed onto GIC. Despite multiple spikes in the electrochemical oxidation reactor, PFOS could be removed completely, whereas PFOA can be reduced to about 500 ng/L. PFBS could be degraded as a by-product of PFOS degradation suggesting that it involved attacks by aqueous electrons on GIC flakes instead of hydroxyl radicals attack in the bulk. On the other hand, no significant removal of PFBS took place when spiked individually. When these 3 PFAS were spiked together, the PFOS and PFOA final concentration was still 1–2 µg/L. With regards to breakdown by-products, the final concentration remained below 300 ng/L. GIC seems inefficient towards smaller PFAS once they reach concentrations lower than 200 ng/L. Tests in real water matrix showed a drop in removal between 3 and 40 % for PFOS, PFOA and smaller sulfonates compared to tap water. This hybrid approach may offer benefits such as rapid removal of PFAS from µg/L to ng/L, potential treatment of a wider range of PFAS compounds, and the possibility of reducing the volume of waste generated compared to individual treatment methods, but more work should be done on smaller PFAS and novel conductive adsorbent targeting them.

Ethical approval

Not Applicable.

Consent to participate

Not Applicable.

Consent to publish

All authors consent to publish in Environmental Science and Pollution Research.

Funding

The authors thank the Japan Society for the Promotion of Science (JSPS) for a long-term invitational fellowship awarded to Dr. Antoine Trzcinski (fellowship ID L21554).

CRediT authorship contribution statement

Antoine P. Trzcinski: Writing – original draft, Investigation,

Funding acquisition, Formal analysis, Data curation, Conceptualization. **Kouji H. Harada:** Writing – review & editing, Validation, Supervision, Software, Resources, Project administration, Methodology, Funding acquisition.

Declaration of competing interest

The authors declare no potential conflict of interest regarding the publication of this work. In addition, the ethical issues including plagiarism, informed consent, misconduct, data fabrication and, or falsification, double publication and, or submission, and redundancy have been completely witnessed by the authors.

Data availability

all data are provided in the manuscript

Acknowledgements

The authors would like to thank Matt Wolski for kindly providing the Daramic membrane used in this research.

Appendix A. Supplementary data

Supplementary data to this article can be found online at https://doi.org/10.1016/j.scitotenv.2024.172184.

References

Ambaye, T.G., Vaccari, M., Prasad, S., Rtimi, S., 2022. Recent progress and challenges on the removal of per- and poly-fluoroalkyl substances (PFAS) from contaminated soil and water. Environ. Sci. Pollut. Res. 29, 58405–58428.
Askeland, M., Clarke, B.O., Cheema, S.A., Mendez, A., Gasco, G., Paz-Ferreiro, J., 2020. Biochar sorption of PFOS, PFOA, PFHxS and PFHxA in two soils with contrasting texture. Chemosphere 249, 126072.
Barisci, S., Suri, R., 2020. Electrooxidation of short and long chain perfluorocarboxylic acids using boron doped diamond electrodes. Chemosphere 243, 125349.
Bentel, M.J., Yu, Y., Xu, L., Li, Z., Wong, B.M., Men, Y., Liu, J., 2019. Defluorination of per- and Polyfluoroalkyl substances (PFASs) with hydrated electrons: structural dependence and implications to PFAS remediation and management. Environ. Sci. Technol. 53, 3718–3728.
Cheng, J., Vecitis, C.D., Park, H., Mader, B.T., Hoffmann, M.R., 2008. Sonochemical degradation of perfluorooctane sulfonate (PFOS) and perfluorooctanoate (PFOA) in landfill groundwater: environmental matrix effects. Environ. Sci. Technol. 42, 8057–8063.
Chou, Y.-C., Lo, S.-L., Kuo, J., Yeh, C.-J., 2013. A study on microwave oxidation of landfill leachate—contributions of microwave-specific effects. J. Hazard. Mater. 246-247, 79–86.
Cui, D., Li, X., Quinete, N., 2020. Occurrence, fate, sources and toxicity of PFAS: what we know so far in Florida and major gaps. TrAC Trends Anal. Chem. 130, 115976.
Dadashi Firouzjaei, M., Zolghadr, E., Ahmadalipour, S., Taghvaei, N., Akbari Afkhami, F., Nejati, S., Elliott, M.A., 2022. Chemistry, abundance, detection and treatment of per- and polyfluoroalkyl substances in water: a review. Environ. Chem. Lett. 20, 661–679.
Deng, S., Nie, Y., Du, Z., Huang, Q., Meng, P., Wang, B., Huang, J., Yu, G., 2015. Enhanced adsorption of perfluorooctane sulfonate and perfluorooctanoate by bamboo-derived granular activated carbon. J. Hazard. Mater. 282, 150–157.
Deng, Y., Liang, Z., Lu, X., Chen, D., Li, Z., Wang, F., 2021. The degradation mechanisms of perfluorooctanoic acid (PFOA) and perfluorooctane sulfonic acid (PFOS) by different chemical methods: a critical review. Chemosphere 283, 131168.
Du, Z., Deng, S., Bei, Y., Huang, Q., Wang, B., Huang, J., Yu, G., 2014. Adsorption behavior and mechanism of perfluorinated compounds on various adsorbents—a review. J. Hazard. Mater. 274, 443–454.
Duinslaeger, N., Radjenovic, J., 2022. Electrochemical degradation of per- and polyfluoroalkyl substances (PFAS) using low-cost graphene sponge electrodes. Water Res. 213, 118148.
EPA, U., 2016. Drinking water health advisory for perfluorooctane sulfonate (PFOS). Office of Water (4304T), Health and Ecological Criteria Division EPA.
EPA, U., 2022. Drinking Water Health Advisories for PFOA, PFOS, GenX Chemicals and PFBS. Office of Water (4304T), Health and Ecological Criteria Division EPA.
Gu, Y., Dong, W., Luo, C., Liu, T., 2016. Efficient reductive decomposition of perfluorooctanesulfonate in a high photon flux UV/sulfite system. Environ. Sci. Technol. 50, 10554–10561.
Hao, S., Choi, Y.-J., Wu, B., Higgins, C.P., Deeb, R., Strathmann, T.J., 2021. Hydrothermal alkaline treatment for destruction of per-and polyfluoroalkyl substances in aqueous film-forming foam. Environ. Sci. Technol. 55, 3283–3295.
Harada, K., Xu, F., Ono, K., Iijima, T., Koizumi, A., 2005. Effects of PFOS and PFOA on L-type Ca2+ currents in guinea-pig ventricular myocytes. Biochem. Biophys. Res. Commun. 329, 487–494.
Harada, K.H., Fujii, Y., Zhu, J., Zheng, B., Cao, Y., Hitomi, T., 2020. Analysis of Perfluorooctanesulfonate Isomers and Other Perfluorinated Alkyl Acids in Serum by In-Port Arylation Gas Chromatography Negative Chemical Ionization–Mass Spectrometry. Env. Sci. Technol. Lett. 7, 259–265.
Harrad, S., Wemken, N., Drage, D.S., Abdallah, M.A.-E., Coggins, A.-M., 2019. Perfluoroalkyl substances in drinking water, indoor air and dust from Ireland: implications for human exposure. Environ. Sci. Technol. 53, 13449–13457.
Isowamwen, O., Li, R., Holsen, T., Thagard, S.M., 2023. Plasma-assisted degradation of a short-chain perfluoroalkyl substance (PFAS): Perfluorobutane sulfonate (PFBS). J. Hazard. Mater. 456, 131691.
Kim, K.Y., Ekpe, O.D., Lee, H.-J., Oh, J.-E., 2020. Perfluoroalkyl substances and pharmaceuticals removal in full-scale drinking water treatment plants. J. Hazard. Mater. 400, 123235.
Kothawala, D.N., Köhler, S.J., Östlund, A., Wiberg, K., Ahrens, L., 2017. Influence of dissolved organic matter concentration and composition on the removal efficiency of perfluoroalkyl substances (PFASs) during drinking water treatment. Water Res. 121, 320–328.
Le, T.X.H., Haflich, H., Shah, A.D., Chaplin, B.P., 2019. Energy-efficient electrochemical oxidation of perfluoroalkyl substances using a Ti4O7 reactive electrochemical membrane anode. Environ. Sci. Technol. Lett. 6, 504–510.
Lee, Y.-C., Lo, S.-L., Chiueh, P.-T., Chang, D.-G., 2009. Efficient decomposition of perfluorocarboxylic acids in aqueous solution using microwave-induced persulfate. Water Res. 43, 2811–2816.
Lei, Y.-J., Tian, Y., Sobhani, Z., Naidu, R., Fang, C., 2020. Synergistic degradation of PFAS in water and soil by dual-frequency ultrasonic activated persulfate. Chem. Eng. J. 388, 124215.
Lei, X., Lian, Q., Zhang, X., Wang, T., Gee, M., Holmes, W., Jin, S., Ponnusamy, S.K., Gang, D.D., Zappi, M.E., 2022. Removal of perfluorooctanoic acid via polyethyleneimine modified graphene oxide: effects of water matrices and understanding mechanisms. Chemosphere 308, 136379.
Leung, S.C.E., Shukla, P., Chen, D., Eftekhari, E., An, H., Zare, F., Ghasemi, N., Zhang, D., Nguyen, N.-T., Li, Q., 2022. Emerging technologies for PFOS/PFOA degradation and removal: a review. Sci. Total Environ. 827, 153669.
Li, X., Chen, S., Quan, X., Zhang, Y., 2011. Enhanced adsorption of PFOA and PFOS on multiwalled carbon nanotubes under electrochemical assistance. Environ. Sci. Technol. 45, 8498–8505.
Li, Y., Lv, L., Yang, L., He, L., Chen, Y., Wu, L., Zhang, Z., 2023. Boosting degradation and defluorination efficiencies of PFBS in a vacuum-ultraviolet/S(IV) process with iodide involvement. Chemosphere 313, 137531.
Liang, S., Pierce Jr., R.D., Lin, H., Chiang, S.Y., Huang, Q.J., 2018. Electrochemical oxidation of PFOA and PFOS in concentrated waste streams. Remediation 28, 127–134.
Liao, Z., Farrell, J., 2009. Electrochemical oxidation of perfluorobutane sulfonate using boron-doped diamond film electrodes. J. Appl. Electrochem. 39, 1993–1999.
Lin, A.Y.-C., Panchangam, S.C., Chang, C.-Y., Hong, P.K.A., Hsueh, H.-F., 2012. Removal of perfluorooctanoic acid and perfluorooctane sulfonate via ozonation under alkaline condition. J. Hazard. Mater. 243, 272–277.
Lin, J.-C., Hu, C.-Y., Lo, S.-L., 2016. Effect of surfactants on the degradation of perfluorooctanoic acid (PFOA) by ultrasonic (US) treatment. Ultrason. Sonochem. 28, 130–135.
Lyu, X.-J., Li, W.-W., Lam, P.K., Yu, H.-Q., 2015. Boiling significantly promotes photodegradation of perfluorooctane sulfonate. Chemosphere 138, 324–327.
Maldonado, V.Y., Landis, G.M., Ensch, M., Becker, M.F., Witt, S.E., Rusinek, C.A., 2021. A flow-through cell for the electrochemical oxidation of perfluoroalkyl substances in landfill leachates. J. Water Process Eng. 43, 102210.
Mohammed, F.M., Roberts, E.P.L., Hill, A., Campen, A.K., Brown, N.W., 2011. Continuous water treatment by adsorption and electrochemical regeneration. Water Res. 45, 3065–3074.
Mohammed, F.M., Roberts, E.P., Campen, A.K., Brown, N.W., 2012. Wastewater treatment by multi-stage batch adsorption and electrochemical regeneration. J. Electrochem. Sci. Eng. 2, 223–236.
Mojiri, A., Zhou, J.L., Ozaki, N., KarimiDermani, B., Razmi, E., Kasmuri, N., 2023. Occurrence of per- and polyfluoroalkyl substances in aquatic environments and their removal by advanced oxidation processes. Chemosphere 330, 138666.
Moriwaki, H., Takagi, Y., Tanaka, M., Tsuruho, K., Okitsu, K., Maeda, Y., 2005. Sonochemical decomposition of perfluorooctane sulfonate and perfluorooctanoic acid. Environ. Sci. Technol. 39, 3388–3392.
Niu, J., Lin, H., Xu, J., Wu, H., Li, Y., 2012. Electrochemical mineralization of perfluorocarboxylic acids (PFCAs) by Ce-doped modified porous nanocrystalline PbO2 film electrode. Environ. Sci. Technol. 46, 10191–10198.
Ohno, M., Ito, M., Ohkura, R., Kose, T., Okuda, T., Nakai, S., Kawata, K., Nishijima, W., 2014. Photochemical decomposition of perfluorooctanoic acid mediated by iron in strongly acidic conditions. J. Hazard. Mater. 268, 150–155.
Pierpaoli, M., Szopińska, M., Wilk, B.K., Sobaszek, M., Łuczkiewicz, A., Bogdanowicz, R., Fudala-Książek, S., 2021. Electrochemical oxidation of PFOA and PFOS in landfill leachates at low and highly boron-doped diamond electrodes. J. Hazard. Mater. 403, 123606.
Pinkard, B.R., Shetty, S., Stritzinger, D., Bellona, C., Novosselov, I.V., 2021. Destruction of perfluorooctanesulfonate (PFOS) in a batch supercritical water oxidation reactor. Chemosphere 279, 130834.
Qu, Y., Zhang, C., Li, F., Chen, J., Zhou, Q., 2010. Photo-reductive defluorination of perfluorooctanoic acid in water. Water Res. 44, 2939–2947.

Radjenovic, J., Duinslaeger, N., Avval, S.S., Chaplin, B.P., 2020. Facing the challenge of poly-and perfluoroalkyl substances in water: is electrochemical oxidation the answer? Environ. Sci. Technol. 54, 14815–14829.
Sharma, D., CF Forster, C., 1996. Removal of hexavalent chromium from aqueous solutions by granular activated carbon. Water SA 22, 153–160.
Stoiber, T., Evans, S., Temkin, A.M., Andrews, D.Q., Naidenko, O.V., 2020. PFAS in drinking water: an emergent water quality threat. Water Sol. 1, e49.
Sukmilin, A., Sangsirimongkolying, R., 2021. Treatment of iron from groundwater by ozonation: influence of hardness as a scavenger. Appl. Environ. Res. 43, 106–115.
Sundström, M., Bogdanska, J., Pham, H.V., Athanasios, V., Nobel, S., McAlees, A., Eriksson, J., DePierre, J.W., Bergman, Å., 2012. Radiosynthesis of perfluorooctanesulfonate (PFOS) and perfluorobutanesulfonate (PFBS), including solubility, partition and adhesion studies. Chemosphere 87, 865–871.
Szabo, J., Hall, J., Magnuson, M., Panguluri, S., Meiners, G., 2017. Treatment of Perfluorinated Alkyl Substances in Wash Water Using Granular Activated Carbon and Mixed Media. in: Washington, D., EPA/600/R-17/175, 2017 (Ed.). US EPA report.
Tang, C.Y., Fu, Q.S., Robertson, A.P., Criddle, C.S., Leckie, J.O., 2006. Use of reverse osmosis membranes to remove perfluorooctane sulfonate (PFOS) from semiconductor wastewater. Environ. Sci. Technol. 40, 7343–7349.
Tenorio, R., Liu, J., Xiao, X., Maizel, A., Higgins, C.P., Schaefer, C.E., Strathmann, T.J., 2020. Destruction of per- and polyfluoroalkyl substances (PFASs) in aqueous film-forming foam (AFFF) with UV-sulfite photoreductive treatment. Environ. Sci. Technol. 54, 6957–6967.
Thompson, J., Eaglesham, G., Mueller, J., 2011. Concentrations of PFOS, PFOA and other perfluorinated alkyl acids in Australian drinking water. Chemosphere 83, 1320–1325.
Trzcinski, A.P., Harada, K., 2023. Adsorption of PFOS onto graphite intercalated compound and analysis of degradation by-products during electro-chemical oxidation. Chemosphere 323, 138268.
Trzcinski, A.P., Ofoegbu, N., Stuckey, D.C., 2011. Post-treatment of the permeate of a submerged anaerobic membrane bioreactor (SAMBR) treating landfill leachate. J. Env. Sci. Health, Part A 46, 1539–1548.
Vecitis, C.D., Park, H., Cheng, J., Mader, B.T., Hoffmann, M.R., 2009. Treatment technologies for aqueous perfluorooctanesulfonate (PFOS) and perfluorooctanoate (PFOA). Front. Env. Sci. Eng. China 3, 129–151.
Wang, F., Shih, K., Leckie, J.O., 2015. Effect of humic acid on the sorption of perfluorooctane sulfonate (PFOS) and perfluorobutane sulfonate (PFBS) on boehmite. Chemosphere 118, 213–218.
Wang, Y., Shi, H., Li, C., Huang, Q., 2020. Electrochemical degradation of perfluoroalkyl acids by titanium suboxide anodes. Environ. Sci.: Water Res. Technol. 6, 144–152.
Xia, C., Lim, X., Yang, H., Goodson, B.M., Liu, J., 2022. Degradation of per- and polyfluoroalkyl substances (PFAS) in wastewater effluents by photocatalysis for water reuse. J. Water Process Eng. 46, 102556.
Yan, H., Cousins, I.T., Zhang, C., Zhou, Q., 2015. Perfluoroalkyl acids in municipal landfill leachates from China: occurrence, fate during leachate treatment and potential impact on groundwater. Sci. Total Environ. 524, 23–31.
Yue, Y., Li, S., Qian, Z., Pereira, R.F., Lee, J., Doherty, J.J., Zhang, Z., Peng, Y., Clark, J. M., Timme-Laragy, A.R., 2020. Perfluorooctanesulfonic acid (PFOS) and perfluorobutanesulfonic acid (PFBS) impaired reproduction and altered offspring physiological functions in Caenorhabditis elegans. Food Chem. Toxicol. 145, 111695.
Zhang, C., Jiang, Y., Li, Y., Hu, Z., Zhou, L., Zhou, M., 2013. Three-dimensional electrochemical process for wastewater treatment: a general review. Chem. Eng. J. 228, 455–467.
Zhang, D., Luo, Q., Gao, B., Chiang, S.-Y.D., Woodward, D., Huang, Q., 2016. Sorption of perfluorooctanoic acid, perfluorooctane sulfonate and perfluoroheptanoic acid on granular activated carbon. Chemosphere 144, 2336–2342.
Zhang, J., Zhang, H., Liu, X., Cui, F., Zhao, Z., 2022. Efficient reductive and oxidative decomposition of haloacetic acids by the vacuum-ultraviolet/sulfite system. Water Res. 210, 117974.